nature neuroscience

Inhibition of inhibition in visual cortex: the logic of connections between molecularly distinct interneurons

Carsten K Pfeffer[1,2], Mingshan Xue[2], Miao He[3], Z Josh Huang[3] & Massimo Scanziani[1,2]

Cortical inhibitory neurons contact each other to form a network of inhibitory synaptic connections. Our knowledge of the connectivity pattern underlying this inhibitory network is, however, still incomplete. Here we describe a simple and complementary interaction scheme between three large, molecularly distinct interneuron populations in mouse visual cortex: parvalbumin-expressing interneurons strongly inhibit one another but provide little inhibition to other populations. In contrast, somatostatin-expressing interneurons avoid inhibiting one another yet strongly inhibit all other populations. Finally, vasoactive intestinal peptide–expressing interneurons preferentially inhibit somatostatin-expressing interneurons. This scheme occurs in supragranular and infragranular layers, suggesting that inhibitory networks operate similarly at the input and output of the visual cortex. Thus, as the specificity of connections between excitatory neurons forms the basis for the cortical canonical circuit, the scheme described here outlines a standard connectivity pattern among cortical inhibitory neurons.

Synaptic inhibition orchestrates both spontaneous and sensory-driven activity in the cerebral cortex[1]. Cortical inhibition is generated by a variety of molecularly distinct types of GABAergic neurons, also referred to as interneurons[2–5]. These neurons are an integral part of the cortical circuit, as they reciprocally connect to other cortical neurons[1]. Although much of the effort in understanding the functional impact of cortical interneurons has focused on their interaction with excitatory neurons, several anatomical and electrophysiological studies have also described interconnections between neocortical interneurons[6–18]. That is, interneurons are embedded in an inhibitory network that is likely to be instrumental in regulating their activity.

The current picture of the connectivity between cortical interneurons, however, is still incomplete mainly because of ambiguities in their categorization. Anatomical studies, for example, have categorized interneurons based on morphological and/or molecular criteria[6–9]. The lack of a clear relationship between morphological and molecular characteristics[4,5,19] precludes a general overview of the connectivity between cortical interneurons.

Transgenic mouse lines expressing fluorescent proteins or Cre recombinase in a variety of different cortical neurons are becoming an essential tool for studying cortical connectivity since they provide a consistent classification of cell populations across experiments and laboratories. Analyses of transgenic mouse lines with labeled subpopulations of interneurons have indeed contributed, in combination with paired electrophysiological recordings, to the understanding of important aspects of connectivity among cortical interneurons[11–13,17,18].

Here we used interneuron-specific *Cre* driver lines (here referred to as Cre lines)[20,21] and optogenetic stimulation[22] to activate genetically defined presynaptic interneurons. We recorded postsynaptic GABAergic currents from interneurons that we categorized using single-cell molecular profiling[23]. Thus, Cre lines allowed us to consistently activate the same genetically defined population of neurons throughout experiments, and the molecular profiling allowed us to simply and reliably categorize interneurons based on the expression of a few genes. With this combination of techniques, we revealed the blueprint through which the three largest and non-overlapping classes of molecularly distinct interneurons in mouse visual cortex[24] interact among each other and with other cortical interneurons. We found that in cortical layers 2/3 and 5 (L2/3 and L5), interneurons expressing parvalbumin (Pvalb), somatostatin (Sst) and vasoactive intestinal peptide (Vip) interacted via a simple and complementary connectivity scheme. Pvalb-expressing cells preferentially inhibited one another, Sst-expressing cells avoided one another and inhibited all other types of interneurons, and Vip-expressing cells preferentially inhibited Sst-expressing cells. Thus, the molecular identity of an interneuron predicts its connectivity within the network, which validates the use of the genetic expression pattern as a criterion for the functional categorization of cell types. Our data establish a standard connectivity pattern between molecularly distinct interneurons in L2/3 and L5 of mouse visual cortex.

RESULTS

Defining the three presynaptic populations

We used three mouse Cre lines (referred to as Pvalb-Cre, Sst-Cre and Vip-Cre cells; Online Methods) to drive expression of channelrhodopsin 2 (ChR2). This allowed us to photoactivate three genetically defined 'presynaptic' populations of interneurons. These three lines expressed Cre recombinase in three largely non-overlapping populations of interneurons that, together, represent ~80% of interneurons in the primary visual cortex. We determined the overlap

[1]Howard Hughes Medical Institute, University of California San Diego, La Jolla, California, USA. [2]Center for Neural Circuits and Behavior, Neurobiology Section and Department of Neuroscience, University of California San Diego, La Jolla, California, USA. [3]Cold Spring Harbor Laboratory, Cold Spring Harbor, New York, USA. Correspondence should be addressed to C.K.P. (cpfeffer10@gmail.com) or M.S. (massimo@ucsd.edu).

Received 4 April; accepted 21 May; published online 30 June 2013; doi:10.1038/nn.3446

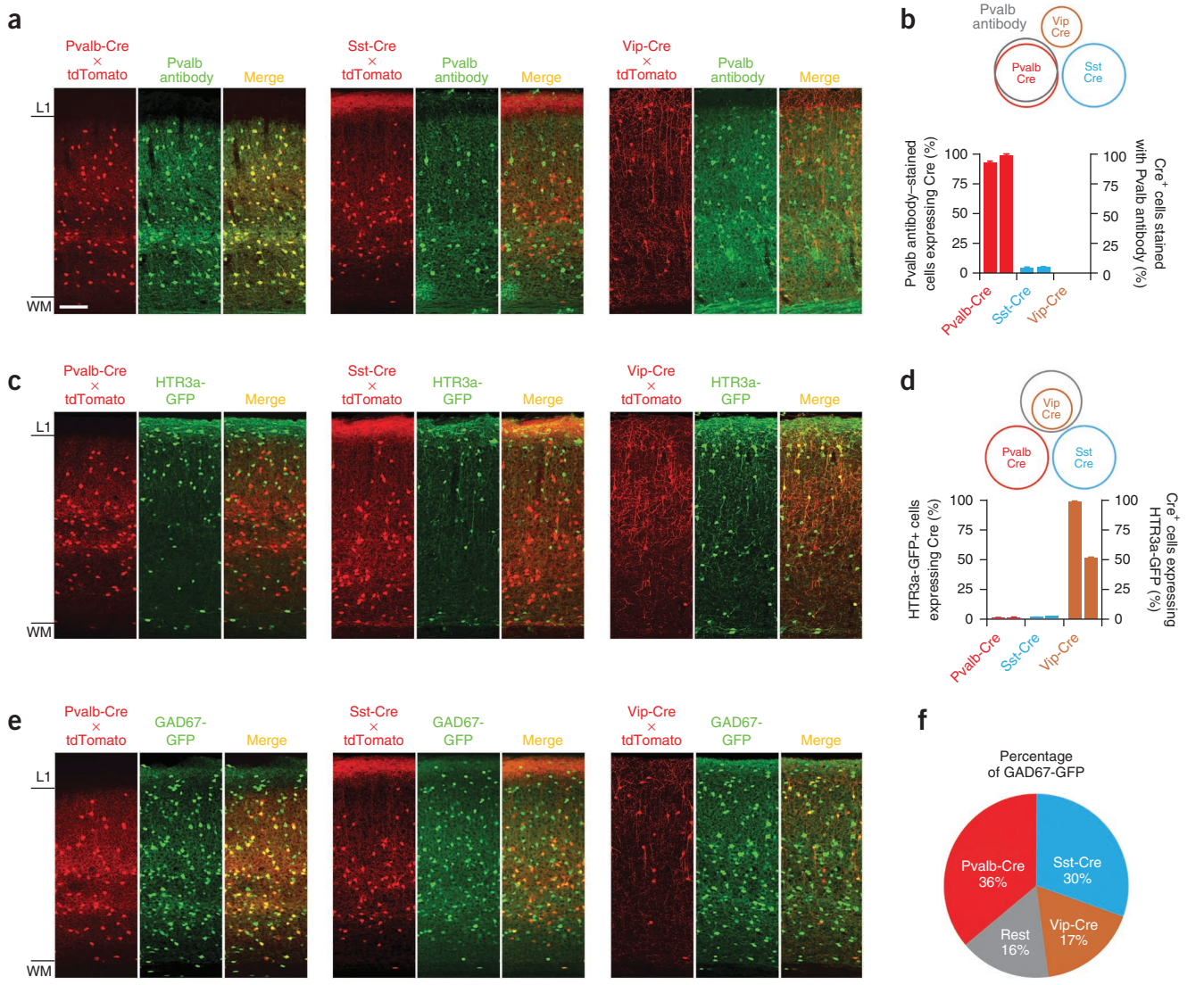

Figure 1 Three non-overlapping Cre lines. (**a**) Confocal fluorescence images of coronal sections through visual cortex of Pvalb-Cre (left), Sst-Cre (center) and Vip-Cre (right) lines showing Cre expression (revealed by crossing the Cre lines with the *ROSA-tdTomato* reporter line; Pvalb-Cre × tdTomato) counterstaining with Pvalb antibody and overlay (merge). Note labeling of Pvalb-Cre cells but not Sst-Cre or Vip-Cre cells with Pvalb antibodies. WM, white matter. (**b**) Schematic of overlap of Cre lines with respect to Pvalb antibody labeling (top) and quantification of overlap (bottom). Left and right ordinates refer to left and right data columns for each Cre line, respectively. Error bars, s.e.m. (Pvalb: $n = 1{,}548$ cells, 4 sections, 2 mice; Sst: $n = 1{,}933$ cells, 6 sections, 2 mice; Vip: $n = 1{,}465$ cells, 6 sections, 2 mice). (**c**) Confocal fluorescence images as in **a** of the three Cre lines crossed with the *Htr3a-GFP* line. Note labeling of Vip-Cre cells with GFP, but not of Pvalb-Cre or Sst-Cre cells with GFP. (**d**) Schematic of overlap of Cre lines with cells labeled in the *Htr3a-GFP* line (top) and quantification of overlap (bottom), as in **b**. Error bars, s.e.m. (Pvalb: $n = 1{,}373$ cells, 4 sections, 2 mice; Sst: $n = 1{,}666$ cells, 4 sections, 2 mice; Vip: $n = 1{,}243$ cells, 4 sections, 2 mice). (**e**) Confocal fluorescence images as in **a** of the three Cre lines crossed with the *Gad67-GFP* line. (**f**) Overlap of Cre lines with cells labeled in the *Gad67-GFP* line. (Pvalb: overlap = 36.2 ± 0.5 s.e.m., $n = 1{,}548$ cells, 4 sections, 2 mice; Sst: overlap = 30.4 ± 1.5 s.e.m., $n = 3{,}869$, 6 sections, 2 mice; Vip: overlap = 17.4 ± 1 s.e.m., $n = 3{,}033$ cells, 6 sections, 2 mice). Scale bar, 100 μm (**a**,**c**,**e**).

between these three Cre recombinase–expressing populations by performing cross-comparisons between their Cre expression pattern and patterns of independent immunohistochemical or genetic markers of GABAergic interneurons. We visualized Cre expression using a tdTomato reporter. Staining with antibody to Pvalb almost exclusively labeled Pvalb-Cre cells (93% ± 0.6% (± s.e.m.) of cells stained with the Pvalb antibody expressed Cre recombinase; 99% ± 0.2% of Pvalb-Cre–expressing cells were stained with Pvalb antibody; **Fig. 1a**,**b**). In contrast, Pvalb antibody did not label Sst-Cre–expressing cells (4% ± 0.3% Pvalb antibody–labeled cells expressed Cre recombinase; 5% ± 0.5% Cre-expressing cells were labeled with Pvalb antibody; **Fig. 1a**,**b**) or Vip-Cre–expressing cells (0%; **Fig. 1a**,**b**). These data indicate that the overlap between the Pvalb-Cre and the Sst-Cre and Vip-Cre populations was maximally 6% and 1%, respectively (this upper bound was calculated by assuming that all Pvalb-Cre cells that were not stained by the Pvalb antibody (1%) were shared with the other two Cre lines, and that all Sst-Cre cells labeled with a Pvalb antibody (5%) were shared with the Pvalb-Cre line).

To determine the overlap between the Vip-Cre cells and the two other populations, we used a different strategy because anti-Vip immunostaining was unreliable in our hands. Because of the reported large overlap between the expression of Vip and 5-HT3A receptor

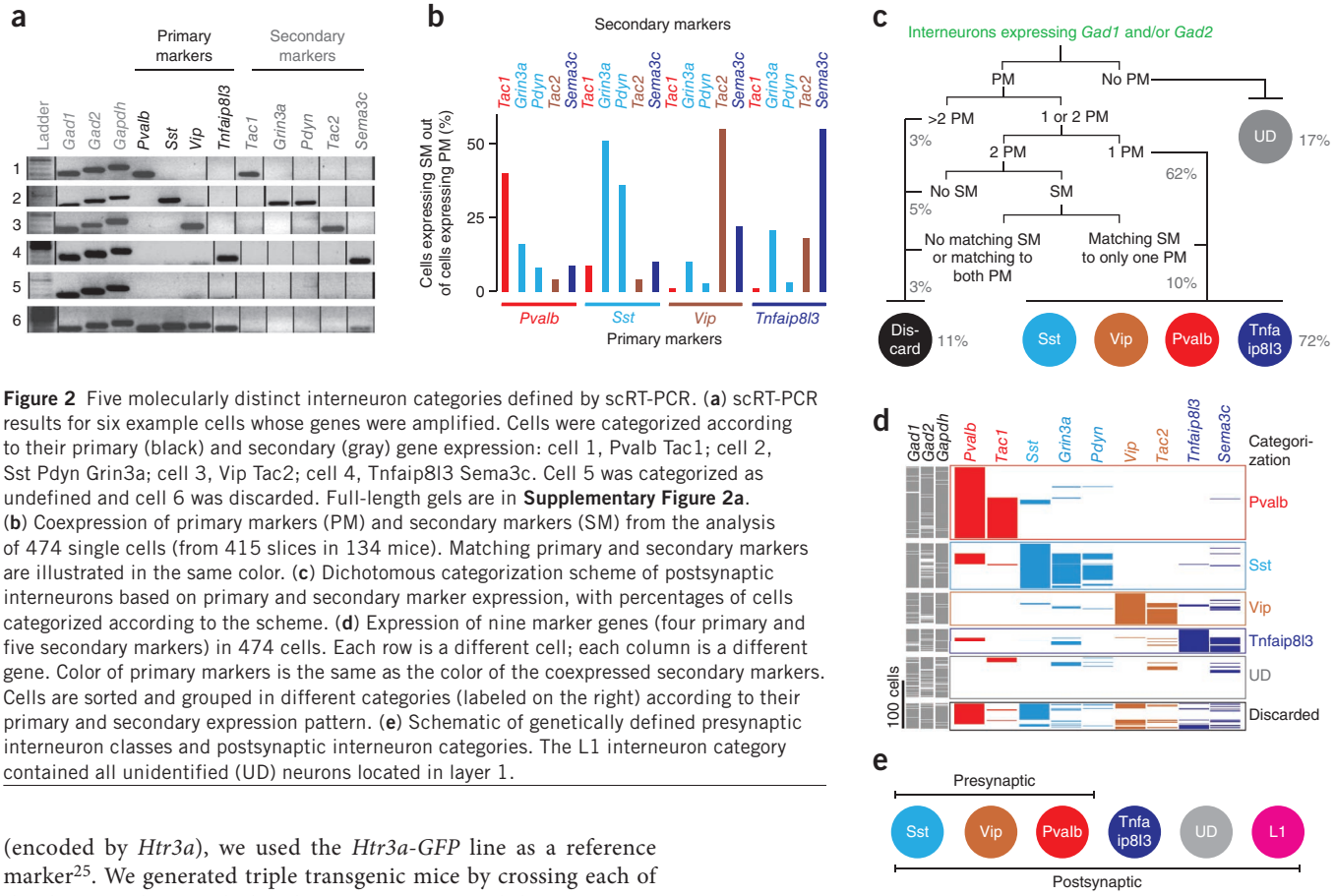

Figure 2 Five molecularly distinct interneuron categories defined by scRT-PCR. (**a**) scRT-PCR results for six example cells whose genes were amplified. Cells were categorized according to their primary (black) and secondary (gray) gene expression: cell 1, Pvalb Tac1; cell 2, Sst Pdyn Grin3a; cell 3, Vip Tac2; cell 4, Tnfaip8l3 Sema3c. Cell 5 was categorized as undefined and cell 6 was discarded. Full-length gels are in **Supplementary Figure 2a**. (**b**) Coexpression of primary markers (PM) and secondary markers (SM) from the analysis of 474 single cells (from 415 slices in 134 mice). Matching primary and secondary markers are illustrated in the same color. (**c**) Dichotomous categorization scheme of postsynaptic interneurons based on primary and secondary marker expression, with percentages of cells categorized according to the scheme. (**d**) Expression of nine marker genes (four primary and five secondary markers) in 474 cells. Each row is a different cell; each column is a different gene. Color of primary markers is the same as the color of the coexpressed secondary markers. Cells are sorted and grouped in different categories (labeled on the right) according to their primary and secondary expression pattern. (**e**) Schematic of genetically defined presynaptic interneuron classes and postsynaptic interneuron categories. The L1 interneuron category contained all unidentified (UD) neurons located in layer 1.

(encoded by *Htr3a*), we used the *Htr3a-GFP* line as a reference marker[25]. We generated triple transgenic mice by crossing each of the three Cre lines with the tdTomato reporter and the *Htr3a-GFP* line. Virtually all Vip-Cre cells (visualized by expression of tdTomato) also expressed GFP (100%; **Fig. 1c**,**d**), whereas only 52% ± 1% of GFP-expressing cells expressed tdTomato. Thus, the Vip-Cre population is a subpopulation of and is entirely comprised in the HTR3A-GFP–expressing population. In contrast, none of the Pvalb-Cre or Sst-Cre cells also expressed GFP (0.13% ± 0.13% and 1% ± 0.2%, respectively; **Fig. 1c**,**d**). These data show that the Vip-Cre cell population does not overlap with either the Pvalb-Cre population or the Sst-Cre population.

In summary, Pvalb-Cre, Sst-Cre and Vip-Cre cells are largely non-overlapping populations of neurons in the visual cortex.

To determine the fraction of interneurons comprised by each of these three populations, we generated triple transgenic mice by crossing each of the Cre lines with the tdTomato reporter and the *Gad1-GFP* (here referred to as *Gad67-GFP*) line, a line that expresses GFP in all interneurons (**Fig. 1e**). Pvalb-Cre, Sst-Cre and Vip-Cre cells made up 36% ± 0.5%, 30% ± 1.5% and 17% ± 1% of the GAD67-GFP–expressing population (**Fig. 1f**), respectively, each with overlapping but not identical distribution across cortical layers (**Supplementary Fig. 1**). Thus, because the three populations are only marginally overlapping, they comprise, together, ~80% of the total GFP-labeled GABAergic population in the *Gad67-GFP* line.

Defining the six postsynaptic populations

We crossed the Cre lines described above with mouse lines expressing GFP in all or a subset of cortical interneurons (Online Methods). This allowed us to visualize the 'postsynaptic' interneurons in slices of the visual cortex and thus target our electrophysiological recordings. We always determined the genetic identity of the recorded interneurons *post hoc* via single-cell reverse-transcription PCR (scRT-PCR), irrespective of the mouse line used. We sampled the postsynaptic population in L1, L2/3 and L5. To be considered GABAergic, cells had to express at least two of these three genes: *Gapdh* (housekeeping), *Gad1* and *Gad2* (GABA-synthesizing enzymes). We collected 474 interneurons and evaluated them based on the expression of 21 marker genes (**Supplementary Fig. 2a**,**b**). We selected four primary marker genes (*Pvalb*, *Sst*, *Vip* and *Tnfaip8l3*) with largely non-overlapping expression to define four large categories of interneurons. Of all cells, 62% expressed only one of these four markers, and we subdivided them into the following four categories: Pvalb-expressing cells (29%), Sst-expressing cells (14%), Vip-expressing cells (12%) and Tnfaip8l3-expressing cells (7%). A fifth category of interneurons did not express any of the four primary markers, and we labeled them as 'undefined' (UD; 17%). The residual ~21% of the sample comprised cells that expressed more than one primary marker. Could we assign at least some of these cells to one of the four above categories? We discovered that the expression of five additional genes (*Tac1*, *Grin3a*, *Pdyn*, *Tac2* and *Sema3c*), named secondary markers, each correlated strongly with one specific primary marker (*Tac1* with *Pvalb*, *Grin3a* and *Pdyn* with *Sst*, *Tac2* with *Vip*, and *Sema3c* with *Tnfaip8l3*; **Fig. 2a**,**b** and **Supplementary Fig. 2a**,**b**; see refs. 26–28). Thus, we attributed cells expressing two primary markers and a secondary marker matching one of the two primary markers to the matching primary marker category. This allowed us to disambiguate an additional 10% of the cells (**Fig. 2c**). We did not further analyze cells with two primary markers but no matching secondary marker or more than two primary markers (discarded: 11%). Additionally, because the majority of cells recorded in L1 belonged to the undefined category

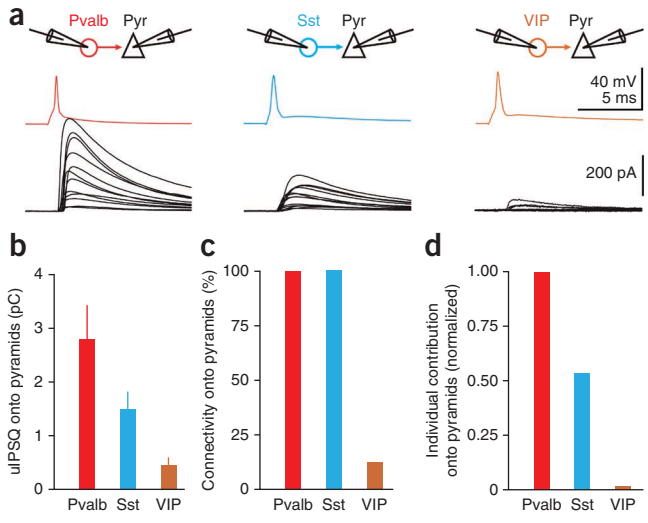

Figure 3 Individual neuronal contributions of the three interneuron classes onto pyramidal cells. (**a**) Schematic of paired recording configuration (top). Average uIPSCs recorded in pyramidal cell (Pyr) in response to an action potential evoked in a defined presynaptic interneuron (bottom). Each trace represents the average postsynaptic current of a different paired recording. Pvalb cells ($n = 12$; 12/12 connected pairs; 5 slices; 3 mice), Sst cells ($n = 12$; 12/12 connected pairs; 6 slices; 2 mice) and Vip cells ($n = 32$; 4/32 connected pairs; 12 slices; 5 mice). (**b**) uIPSQ recorded in pyramidal cell and mediated by the three different presynaptic interneuron classes (Pvalb: $n = 12$; Sst: $n = 12$; Vip: $n = 4$; error bars, s.e.m.). (**c**) Connectivity between the three presynaptic interneuron classes and postsynaptic pyramidal cells. (**d**) Individual neuronal contribution (uIPSQ × P_{con}) of the three presynaptic interneuron classes onto pyramidal cells normalized by the individual neuronal contribution of Pvalb cells. Data in **c** and **d** are calculated from connected pairs in **a** and **b**.

(**Supplementary Fig. 3a**) we defined a specific category for undefined L1 neurons, called L1.

Thus, we classified ~90% of all sampled interneurons into six distinct categories (Pvalb, 30%; Sst, 19%; Vip, 13%; Tnfaip8l3, 10%; undefined, 13%; L1, 4%; **Fig. 2c–e** and **Supplementary Figs. 2c** and **3a**; see Online Methods and **Fig. 2c** for details on categorization).

Finally, we compared the presynaptic interneuron classes defined by Pvalb-Cre, Sst-Cre and Vip-Cre lines with our postsynaptic categorization scheme (we collected cells conditionally expressing the tdTomato reporter). Of the Cre recombinase–expressing neurons, 80% matched the RT-PCR analysis–based categorization (that is, Pvalb-Cre, Sst-Cre and Vip-Cre were categorized as Pvalb-, Sst- and Vip-expressing cells, respectively), 9% of the cells were discarded, 7% were categorized as undefined and only 4% were mismatched (**Supplementary Fig. 3b**), demonstrating that the presynaptic interneuron classes matched our postsynaptic interneuron categorization. We validated our general molecular interneuron categorization by independent principal component analysis, *k*-means clustering and hierarchical tree–based clustering (**Supplementary Figs. 4–6** and Online Methods).

Approach

We photostimulated the ChR2-expressing presynaptic population with a 2-ms full-field light pulse at 470 nm while recording the resulting inhibitory postsynaptic current (IPSC) from postsynaptic interneurons in the voltage-clamp configuration. We recorded in the presence of the AMPA receptor antagonist NBQX (6-nitro-2,3-dioxo-1,4-dihydrobenzo[f]quinoxaline-7-sulfonamide; 5 μM) and of the $GABA_B$ receptor antagonist CGP54626 (1 μM). Because the level of ChR2 expression, the number of ChR2-expressing neurons, the quality of the preparation and the number of action potentials generated through photostimulation may vary across experiments, we performed all recordings from interneurons while simultaneously recording from a neighboring pyramidal cell. By using the IPSC recorded in the pyramidal cell as a reference, we could compare the IPSCs mediated by a given presynaptic interneuron class onto its different postsynaptic targets even if we recorded these in different experimental sessions[29]. Using the pyramidal cell as a reference, however, did not allow us to compare inhibition mediated by the three presynaptic interneuron classes (Pvalb, Sst and Vip) onto the same target category (say, Tnfaip813). This is because the three presynaptic interneuron classes may differ in their connection probability and/or inhibitory response magnitude onto pyramidal cells.

However, if we knew the connectivity, that is, the probability of connection (P_{con}), and the average unitary IPSC (uIPSC) generated by individual Pvalb, Sst and Vip cells onto a pyramidal cell, we could estimate the contribution of each of the three presynaptic interneuron classes onto their various targets, as described below.

We obtained uIPSC and P_{con} data through paired recordings between L2/3 pyramidal cells and nearby Pvalb-Cre, Sst-Cre or Vip-Cre cells (distance, 25–100 μm) visualized by crossing the respective Cre line with the tdTomato reporter line. Pvalb-Cre cells provided the largest unitary inhibitory postsynaptic charge (uIPSQ; the time integral of the uIPSC) onto pyramidal cells (uIPSQ = 2.8 ± 0.64 pC; $n = 12$), followed by Sst-Cre cells (uIPSQ = 1.51 ± 0.3 pC; $n = 12$) and Vip-Cre cells (uIPSQ = 0.47 ± 0.12 pC; $n = 4$; **Fig. 3a**,**b**). In addition, although P_{con} from Pvalb-Cre cells and Sst-Cre cells onto the local pyramidal cells was 100%, consistent with previous reports[30,31], Vip-Cre cells contacted pyramidal cells with only ~12.5% probability (**Fig. 3c**). We defined the individual neuronal contribution (INC) as the product of P_{con} and uIPSQ (INC = uIPSQ × P_{con}). INC thus reports how much inhibition any interneuron of a given class contributes, on average, to any pyramidal cell. The INC for Pvalb-Cre, Sst-Cre and Vip-Cre cells onto pyramidal cells was 2.8 pC, 1.5 pC and 0.06 pC, respectively, and can be given as the normalized ratio Pvalb:Sst:Vip = 1:0.54:0.02, that is, the individual contribution of Vip-Cre cells onto pyramidal cells is 25–50 times less than of Pvalb-Cre or Sst-Cre cells (**Fig. 3d**). We can now normalize the inhibitory charge received by a pyramidal cell ($IPSQ_{Pyr}$) upon photostimulation of a given interneuron class by the INC of that interneuron class, thereby obtaining N_{INC}, that is, the number of INCs generating the $IPSQ_{Pyr}$ ($N_{INC} = IPSQ_{Pyr}/INC$; the number of INCs is related but not necessarily identical to the number of photostimulated interneurons as each interneuron may fire multiple times during photostimulation). By dividing the inhibitory charge simultaneously recorded in the interneuron ($IPSQ_{IN}$) by N_{INC}, we obtain $INC_{INPre \rightarrow INPos}$, that is, the INC of the photostimulated presynaptic interneuron class on the recorded postsynaptic interneuron category ($INC_{INPre \rightarrow INPos} = IPSQ_{IN}/N_{INC}$).

Thus, we can compare inhibition generated by a given presynaptic interneuron class onto distinct postsynaptic categories and by distinct presynaptic inhibitory classes onto a single postsynaptic category.

Interneurons targeted by Pvalb-Cre cells

Photostimulation of Pvalb-Cre cells invariably elicited large IPSQs in L2/3 and L5 pyramidal cells (average IPSQ, 39.3 ± 4.0 pC; $n = 72$ cells), yet the magnitude of inhibition recorded simultaneously in neighboring interneurons varied depending on the genetic profile of the neuron (**Fig. 4a–i**). Only Pvalb-expressing cells received inhibitory charges comparable with those received by pyramidal cells (average $IPSQ_{Pvalb}$,

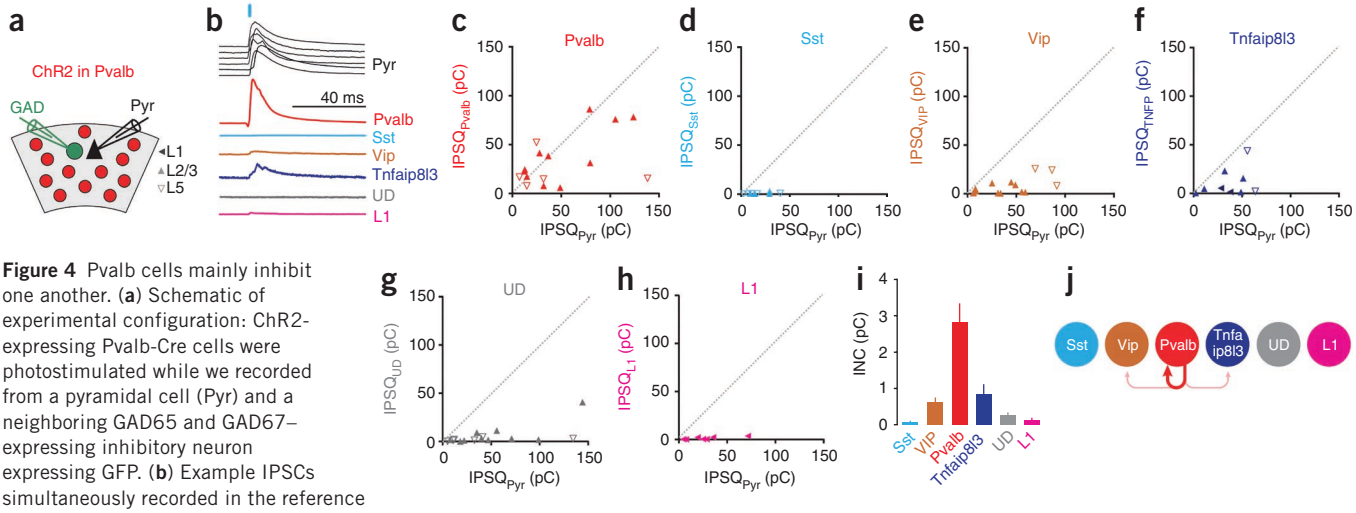

Figure 4 Pvalb cells mainly inhibit one another. (**a**) Schematic of experimental configuration: ChR2-expressing Pvalb-Cre cells were photostimulated while we recorded from a pyramidal cell (Pyr) and a neighboring GAD65 and GAD67–expressing inhibitory neuron expressing GFP. (**b**) Example IPSCs simultaneously recorded in the reference pyramidal cell (black) and in one of the six different interneuron categories. Order of six pyramidal-cell IPSCs (top to bottom) matches the order of the IPSC simultaneously recorded in each of the six interneuron categories. For simplicity, all traces were scaled such that the pyramidal-cell IPSCs have the same peak amplitude. (**c**–**h**) IPSQ evoked by Pvalb cell photostimulation and recorded in individual interneurons versus IPSQ simultaneously recorded in a pyramidal cell ($IPSQ_{Pyr}$; symbols as in **a**). Dotted lines are unity lines. Pvalb: 16 cells, 15 slices, 10 mice; Sst: 9 cells, 9 slices, 6 mice; Vip: 15 cells, 12 slices, 9 mice, Tnfaip8l3: 9 cells, 5 slices, 5 mice; UD: 16 cells, 12 slices, 9 mice: L1: 7 cells, 5 slices, 5 mice. (**i**) Mean ± s.e.m. of INC values of all recorded pairs of the respective category (Sst: 9 cells; Vip: 15 cells; Pvalb: 16 cells; Tnfaip8l3: 9 cells; UD: 16 cells; L1: 7 cells). (**j**) Schematic of the inhibition mediated by Pvalb cells onto each interneuron category.

33.5 ± 6.6 pC; average $IPSQ_{Pyr}$, 49.35 ± 6.6 pC; $n = 16$; $INC_{Pvalb \rightarrow Pvalb}$ = 2.8 ± 0.51 pC; **Fig. 4b**,**c**,**i**). In contrast, Sst-expressing cells were not inhibited at all by Pvalb-Cre cell photostimulation (average $IPSQ_{Sst}$, 0.5 ± 0.3 pC; average $IPSQ_{Pyr}$, 17.7 ± 4.17 pC; $n = 9$; $INC_{Pvalb \rightarrow Sst}$ = 0.07 ± 0.03 pC; **Fig. 4b**,**d**,**i**) and Vip- and Tnfaip813-expressing cells were inhibited only a little (average $IPSQ_{Vip}$, 7.1 ± 2.0 pC; average $IPSQ_{Pyr}$, 38.85 ± 7.57 pC; $n = 15$; $INC_{Pvalb \rightarrow Vip}$, = 0.62 ± 0.14 pC; and average $IPSQ_{TNFA}$, 10.9 ± 2.0 pC; average $IPSQ_{Pyr}$, 36.73 ± 6.86 pC; $n = 9$; $INC_{Pvalb \rightarrow TNFA}$ = 0.85 ± 0.27 pC; **Fig. 4b**,**e**,**f**,**i**; respectively). Similarly, L1 interneurons were not inhibited by Pvalb-Cre cells (average $IPSQ_{L1}$, 1.3 ± 0.5 pC; average $IPSQ_{Pyr}$, 27.02 ± 8.59 pC; $n = 7$; $INC_{Pvalb \rightarrow L1}$ = 0.12 ± 0.04 pC; **Fig. 4b**,**h**,**i**). The undefined cell category was not inhibited by Pvalb-Cre cell photostimulation (average $IPSQ_{UD}$, 5.3 ± 2.5 pC; average $IPSQ_{Pyr}$, 48.52 ± 10.83 pC; $n = 16$; $INC_{Pvalb \rightarrow UD}$ = 0.28 ± 0.07 pC; **Fig. 4b**,**g**,**i**; for statistical significance between groups, see **Supplementary Fig. 7a**).

The lack of inhibition onto the undefined category, which includes most interneurons not defined by genetic markers, indicates that the small inhibition generated by Pvalb-Cre cells onto other interneurons is a general phenomenon.

Thus, these data show that the most prominent category of interneurons in the visual cortex, the Pvalb cell, is selective in its choice of postsynaptic interneuron targets, mainly restricting its inhibitory influence onto itself (**Fig. 4j**).

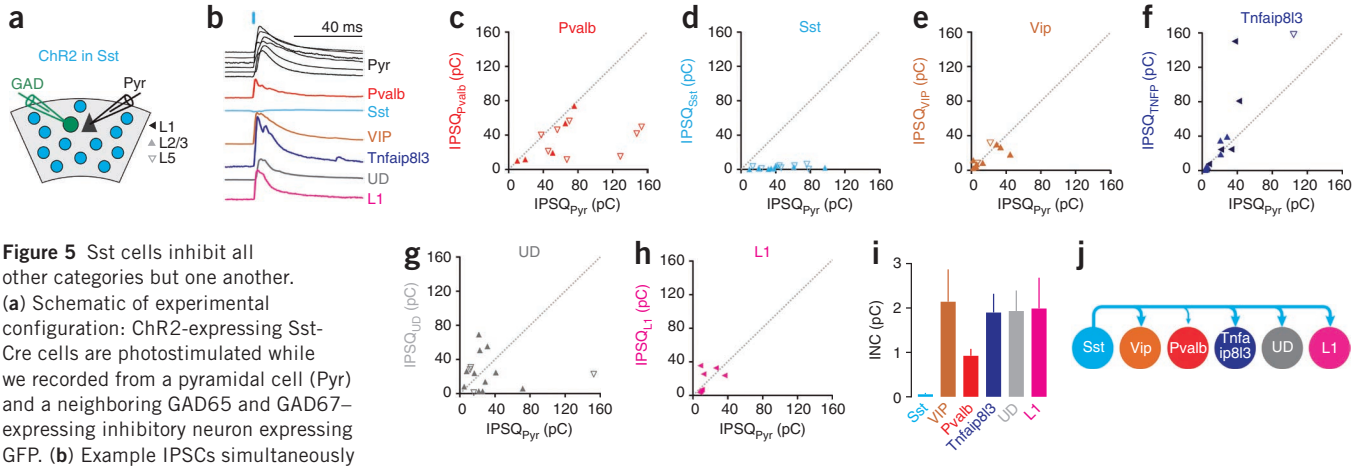

Figure 5 Sst cells inhibit all other categories but one another. (**a**) Schematic of experimental configuration: ChR2-expressing Sst-Cre cells are photostimulated while we recorded from a pyramidal cell (Pyr) and a neighboring GAD65 and GAD67–expressing inhibitory neuron expressing GFP. (**b**) Example IPSCs simultaneously recorded in the reference pyramidal cell (Pyr) and in one of the six different interneuron categories. Order of the six pyramidal-cell IPSCs (top to bottom) matches the order of the IPSC simultaneously recorded in each of the six interneuron categories. All traces were scaled such that the pyramidal-cell IPSCs have the same peak amplitude. (**c**–**h**) IPSQ evoked by Sst cell photostimulation and recorded in individual interneurons versus IPSQ simultaneously recorded in a pyramidal cell ($IPSQ_{Pyr}$; symbols as in **a**). Dotted lines are unity lines. Note that all inhibitory neuron categories received inhibition comparable to that simultaneously recorded in pyramidal cells, but for Sst cells that receive none (**d**). Pvalb: 13 cells, 10 slices, 5 mice; Sst: 12 cells, 6 slices, 5 mice; Vip: 10 cells, 7 slices, 6 mice; Tnfaip8l3: 13 cells, 10 slices, 6 mice; UD: 16 cells, 13 slices, 6 mice; L1: 8 cells, 6 slices, 5 mice. (**i**) Mean ± s.e.m. of INC values of all recorded pairs of the respective category (Sst: 12 cells; Vip: 10 cells; Pvalb: 13 cells; Tnfaip8l3: 13 cells; UD: 16 cells; L1: 8 cells). (**j**) Schematic of the inhibition mediated by Sst cells onto each interneuron category.

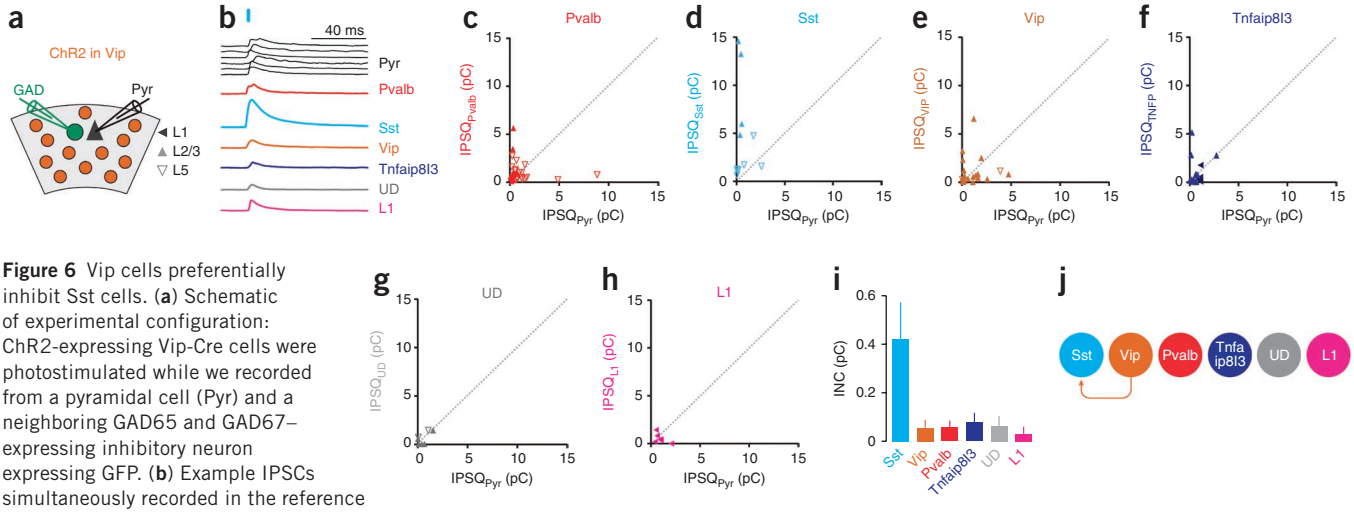

Figure 6 Vip cells preferentially inhibit Sst cells. (**a**) Schematic of experimental configuration: ChR2-expressing Vip-Cre cells were photostimulated while we recorded from a pyramidal cell (Pyr) and a neighboring GAD65 and GAD67–expressing inhibitory neuron expressing GFP. (**b**) Example IPSCs simultaneously recorded in the reference pyramidal cell (Pyr) and in one of the six different interneuron categories. Order of the six pyramidal-cell IPSCs (top to bottom) matches the order of the IPSC simultaneously recorded in each of the six interneuron categories. For simplicity, all traces were scaled such that the pyramidal-cell IPSCs have the same peak amplitude. (**c**–**h**) IPSQ evoked by Vip cell photostimulation and recorded in individual interneurons versus IPSQ simultaneously recorded in a pyramidal cell ($IPSQ_{Pyr}$; symbols as in **a**). Dotted lines are unity lines. Note that only Sst cells received substantial inhibition (**d**). *x* and *y* axes are expanded by one order of magnitude as compared to Pvalb-Cre line (**Fig. 4**) and Sst-Cre line (**Fig. 5**). Category (cells/slices/mice): Pvalb (29/20/12), Sst (11/8/6), Vip (20/14/8), Tnfaip8l3 (18/12/8), UD (7/5/4), L1 (6/5/4). (**i**) Mean ± s.e.m. of INC values of all recorded pairs of the respective category (Sst: 11 cells; Vip: 20 cells; Pvalb: 29 cells; Tnfaip8l3: 18 cells; UD: 7 cells; L1: 6 cells). (**j**) Schematic of the inhibition mediated by Vip cells onto each interneuron category.

Interneurons targeted by Sst-Cre cells

Photostimulation of Sst-Cre-ChR2–expressing neurons showed that Sst-Cre cells, in notable contrast to Pvalb cells, inhibit all other categories of interneurons rather than one another (**Fig. 5a**–**i**). Photostimulation of Sst-Cre cells generated large inhibitory charges in pyramidal cells (average IPSQ, 39.3 ± 4.5 pC; $n = 75$) and charges of comparable magnitude in Pvalb cells (average $IPSQ_{Pvalb}$, 34.6 ± 5.8 pC; average $IPSQ_{Pyr}$, 71.43 ± 12.63 pC; $n = 13$; $INC_{Sst\rightarrow Pvalb} = 0.9 \pm 0.14$ pC; **Fig. 5b**,**c**,**i**), Vip cells (average $IPSQ_{Vip}$, 20.4 ± 6.0 pC; average $IPSQ_{Pyr}$, 21.63 ± 6.0 pC; $n = 10$; $INC_{Sst\rightarrow Vip} = 2.15 \pm 0.72$ pC; **Fig. 5b**,**e**,**i**), Tnfaip813 cells (average $IPSQ_{TNFA}$, 42.3 ± 15.0 pC; average $IPSQ_{Pyr}$, 25.82 ± 7.5 pC; $n = 13$; $INC_{Sst\rightarrow TNFA} = 1.91 \pm 0.41$ pC; **Fig. 5b**,**f**,**i**) and L1 cells (average $IPSQ_{L1}$ 17.4 ± 4.7 pC; average $IPSQ_{Pyr}$, 14.9 ± 3.7 pC; $n = 8$; $INC_{Pvalb\rightarrow L1} = 2.00 \pm 0.69$ pC; **Fig. 5b**,**h**,**i**). Sst-Cre cells also inhibited the undefined category (average $IPSQ_{UD}$, 25.7 ± 5.1 pC; average $IPSQ_{Pyr}$, 42.2 ± 13.3 pC; $n = 16$; $INC_{Pvalb\rightarrow UD} = 1.94 \pm 0.45$ pC; **Fig. 5b**,**g**,**i**), highlighting the general inhibitory impact of Sst-Cre cells onto other interneuron categories. Sst-Cre cells, however, generated no inhibition on Sst-expressing cells (average $IPSQ_{Sst}$, 1.7 ± 0.4 pC; average $IPSQ_{Pyr}$, 45.19 ± 7.3 pC; $n = 12$; $INC_{Sst\rightarrow Sst} = 0.06 \pm 0.01$ pC; **Fig. 5b**,**d**,**i**; for statistical analysis between groups, see **Supplementary Fig. 7b**). Thus, Sst cells exhibited a complementary inhibitory pattern compared to Pvalb cells: the latter preferentially inhibited one another but Sst cells were a major source of inhibition for all other interneuron categories except themselves (**Fig. 5j**).

Interneurons targeted by Vip-Cre cells

As Sst cells were not substantially inhibited by Pvalb cells or by Sst cells, we sought to determine whether any category of interneurons inhibits them. By photostimulating Vip-Cre-ChR2–expressing neurons, we discovered that not only do Vip-Cre cells inhibit Sst cells but that Sst cells are their principal target (**Fig. 6a**–**i**). Inhibition mediated by Vip-Cre cells onto Sst-expressing cells was much larger than onto the simultaneously recorded pyramidal cells (pyramids or Pyr) (average $IPSQ_{Sst}$, 4.6 ± 1.5 pC; average $IPSQ_{Pyr}$, 0.6 ± 0.2 pC; $n = 11$; $INC_{Vip\rightarrow Sst} = 0.42 \pm 0.14$ pC as compared to the much smaller $INC_{Vip\rightarrow pyramid} = 0.06 \pm 0.02$ pC and **Fig. 6b**,**d**,**i**) and larger in L2/3 than in L5, consistent with their preferential distribution in superficial layers (average $IPSQ_{Sst}$, L2/3, 9.7 ± 2.4 pC; average $IPSQ_{Pyr}$ L2/3, 0.4 ± 0.08 pC; $n = 4$; $INC_{Vip\rightarrow SstL2/3} = 1.48 \pm 0.19$ pC; and average $IPSQ_{Sst}$ L5 1.7 ± 0.5 pC; average $IPSQ_{Pyr}$ L5, 0.78 ± 0.4 pC; $n = 7$; $INC_{Vip\rightarrow SstL5} = 0.13 \pm 0.01$ pC; **Fig. 6b**,**d**,**i**; see **Supplementary Figs. 1** and **3a** for layer distribution of cells). In contrast to the inhibition that they generated onto Sst-expressing cells, Vip-Cre cells inhibited all of the other targets very little (average IPSQ values; Pvalb: 1.1 ± 0.2 pC, $pyramid_{Pvalb}$: 1.08 ± 0.32 pC, $n = 29$, $INC_{Vip\rightarrow Pvalb} = 0.06 \pm 0.01$ pC; Vip:1.1 ± 0.3 pC, $pyramid_{Vip}$:1.15 ± 0.3 pC, $n = 20$, $INC_{Vip\rightarrow Vip} = 0.06 \pm 0.02$ pC; Tnfaip8l3:0.9 ± 0.3 pC, $pyramid_{TNFA}$: 0.7 ± 0.14 pC, $n = 18$, $INC_{Vip\rightarrow TNFA} = 0.08 \pm 0.03$ pC; undefined: 0.6 ± 0.2 pC, $pyramid_{UD}$: 0.55 ± 0.22 pC, $n = 7$, $INC_{Vip\rightarrow UD} = 0.07 \pm 0.02$ pC; L1: 0.54 ± 0.2 pC, $pyramid_{L1}$: 0.93 ± 0.25 pC, $n = 6$, $INC_{Vip\rightarrow L1} = 0.03 \pm 0.01$ pC; **Fig. 6b**,**c**,**e**–**i**; for statistical analysis between groups, see **Supplementary Fig. 7c**). Thus, Vip cells exhibited a distinct inhibitory pattern compared to Pvalb and Sst cells. Whereas Pvalb cells preferentially inhibited one another and Sst cells inhibited any other category but one another, Vip cells were specialized in inhibiting Sst cells (**Fig. 6j**).

Comparing inhibition mediated by distinct interneurons

Finally, we compared inhibition between genetically identified interneurons side by side (**Fig. 7a**). For simplicity, we normalized all INCs to the INC between Pvalb and pyramidal cell ($INC_{Pvalb\rightarrow pyramid}$). Normalized INC (nINC) of Pvalb-Cre cells onto Pvalb-expressing cells ($nINC_{Pvalb\rightarrow Pvalb} = 1.01$) was three times that of Sst-Cre cells onto Pvalb-expressing cells ($nINC_{Sst\rightarrow Pvalb} = 0.33$). In contrast, each Sst-Cre cell contributed 2-5 times more to inhibition onto Vip cells, Tnfaip8l3 cells, undefined category and L1 cells as compared to Pvalb-Cre cells ($nINC_{Sst\rightarrow Vip} = 0.77$; $nINC_{Pvalb\rightarrow Vip} = 0.22$; $nINC_{Sst\rightarrow TNFA} = 0.68$; $nINC_{Pvalb\rightarrow TNFA} = 0.3$; $nINC_{Sst\rightarrow UD} = 0.69$; $nINC_{Pvalb\rightarrow UD} = 0.1$; $nINC_{Sst\rightarrow L1} = 0.72$; $nINC_{Pvalb\rightarrow L1} = 0.04$). Finally, Sst-Cre cells

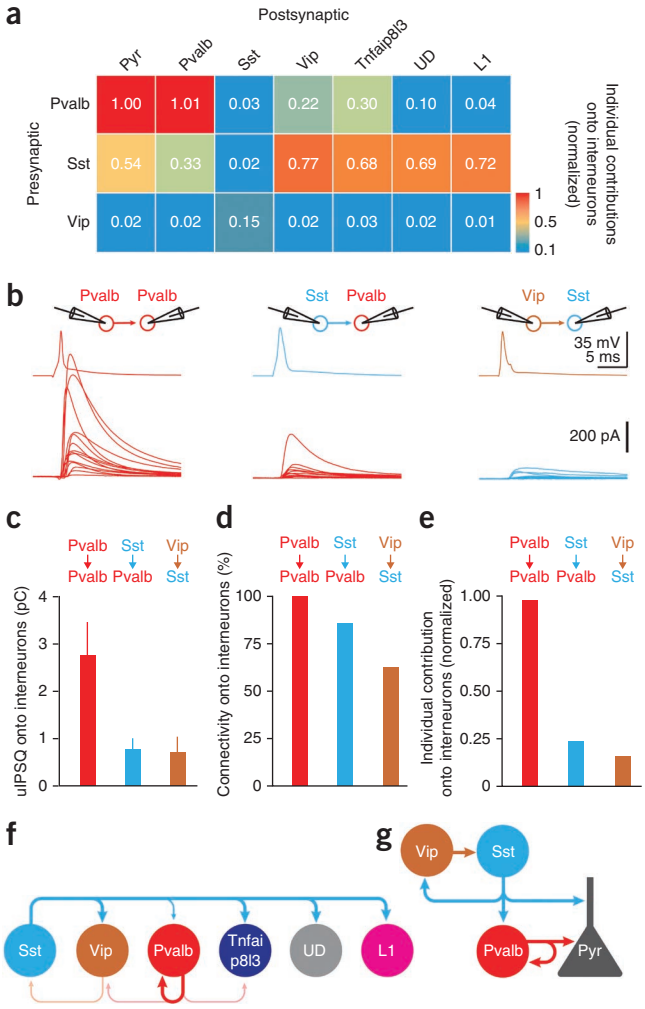

Figure 7 Comparing individual neuronal contributions among cortical interneurons. (**a**) Heat map of the normalized individual neuronal contributions of the three presynaptic interneuron classes onto the six postsynaptic interneuron categories. (**b**) Schematics of paired recording configurations (top). Average uIPSC recorded in pyramidal cells in response to an action potential evoked in a defined presynaptic interneuron (bottom). Each trace represents the average postsynaptic current of a different paired recording. Pvalb onto Pvalb cells (left; $n = 13$; 13/13 connected pairs, 6 slices, 3 mice), Sst onto Pvalb cells (center; $n = 14$; 12/14 connected pairs, 6 slices, 3 mice) and Vip onto Sst cells (right; $n = 16$; 10/16 connected pairs, 7 slices, 3 mice). (**c**) uIPSQs recorded in interneurons and mediated by the three different presynaptic interneuron classes (Pvalb → Pvalb: $n = 13$; Sst → Pvalb: $n = 12$; Vip → Sst: $n = 10$; error bars, s.e.m.). (**d**) Connectivity probability between the three presynaptic interneuron classes and the respective postsynaptic interneurons. (**e**) Individual neuronal contribution (uIPSQ × connectivity probability) of the three presynaptic interneuron classes onto interneurons normalized by the individual neuronal contribution of Pvalb onto pyramidal cells. (**f**) Schematic of the connectivity pattern between the presynaptic interneuron classes (Pvalb, Sst and Vip) and postsynaptic interneuron categories (Pvalb, Sst, Vip, Tnfaip8l3, UD and L1) in L2/3 and L5 of mouse visual cortex (abbreviations as in **Fig. 2e**). (**g**) Schematic of the inhibitory connections among the three largest classes of interneurons (Pvalb, Sst, Vip) and pyramidal cells (abbreviations as in **Fig. 2e**).

received the bulk of the INCs from Vip-Cre cells ($nINC_{Vip\rightarrow Sst} = 0.15$; $nINC_{Pvalb\rightarrow Sst} = 0.03$; $nINC_{Sst\rightarrow Sst} = 0.02$).

Because we computed the INCs listed above indirectly, based on the INCs of interneurons onto pyramidal cells and photostimulation of large populations of interneurons, we directly verified three of the most salient INCs between interneurons, namely $INC_{Pvalb\rightarrow Pvalb}$, $INC_{Sst\rightarrow Pvalb}$ and $INC_{Vip\rightarrow Sst}$, through paired recordings. We obtained uIPSQ and P_{con} data between molecularly identified GFP-expressing interneurons and nearby Pvalb-, Sst- or Vip-Cre cells (distance 25–100 µm) visualized by tdTomato expression in the respective Cre line (**Fig. 7b–e** and Online Methods). Pvalb-Cre cells strongly inhibited Pvalb cells (uIPSQ = 2.76 ± 0.69 pC; $P_{con} = 100\%$; $n = 13$). The $INC_{Pvalb\rightarrow Pvalb}$ obtained with paired recordings (2.76 pC) was very similar to that estimated with photostimulation (2.8 pC; $P = 0.94$). Sst-Cre cells inhibited Pvalb cells (uIPSQ = 0.77 ± 0.21 pC; $n = 12$ $P_{con} = 85.7\%$; $n = 14$) and the $INC_{Sst\rightarrow Pvalb}$ (0.66 pC) was similar to that measured using photostimulation (0.9 pC; $P = 0.58$). Finally, Vip-Cre cells inhibited Sst cells (uIPSQ = 0.69 ± 0.33 pC; $n = 10$; $P_{con} = 62.5\%$; $n = 16$) and the $INC_{Vip\rightarrow Sst}$ (0.43 pC) was again not significantly different than that estimated with photostimulation (0.42 pC; $P = 0.46$). Thus, the results indicate that the two methods, one using photostimulation and normalization onto a reference cell and the other using standard paired recordings, provided quantitatively similar results.

These data show that although Pvalb cells provide little inhibition onto other interneurons, they are the main source of their own inhibition by contributing three times more inhibition than Sst cells do. Furthermore, individual Sst cells contribute much more than individual Pvalb and Vip cells to the inhibition of all other interneuron categories. Finally, although individual Vip cells contributed relatively little inhibition, they still represented the main source of inhibition onto Sst cells (**Fig. 7a,f,g**; for statistical analysis between groups, see **Supplementary Fig. 7d–f**).

DISCUSSION

We established the connectivity pattern between molecularly defined classes of GABAergic interneurons in L2/3 and L5 of the mouse visual cortex. 'Pvalb', 'Sst' and 'Vip' cells exhibited a highly specific and complementary network of connections. Although the biggest group, the Pvalb cells, strongly inhibited each other but weakly other interneurons, the second largest group, the Sst cells, inhibited all interneuron categories but avoided inhibiting each other. Vip cells preferentially targeted Sst cells. This simple blueprint highlights a remarkable degree of specificity in the synaptic interactions between molecularly defined classes of cortical interneurons.

Our data highlight more similarities than differences between L2/3 and L5 inhibitory networks: for example, the strength of the Pvalb-Pvalb and Sst-Pvalb connections, and the lack of Sst-Sst and of Pvalb-Sst connections was comparable across these two layers. The only notable difference was the strength of the Vip-Sst connection, which was larger in L2/3 than in L5, likely due to the concentration of Vip neurons in superficial layers.

Methodological considerations

Although space-clamp errors are inherent to whole-cell voltage-clamp experiments[32], they are unlikely to influence the reported connectivity pattern. They may, however, affect the relative strength of connections, given that distinct interneuron classes preferentially inhibit distinct subcellular compartments. Thus, the inhibition values given here report the strength as experienced by the soma of the recorded neuron rather than at the contact site. The relative connection strength may also be affected by the elimination of subcellular differences in chloride concentrations through whole-cell dialysis, thus abolishing differences in inhibitory driving force at distinct locations.

Although we targeted recordings from interneurons to L1, L2/3 and L5, the photostimulation of the interneuron population was performed in full field. Thus, our data do not allow us to infer the location of the presynaptic interneurons relative to the recorded postsynaptic one.

Comparison with physiological and morphological categories

Cortical interneurons cannot be unequivocally classified based exclusively on physiological or morphological properties, yet rough correlations between these properties and the gene or protein expression pattern of GABAergic interneurons exist[3–5,10,33–38] (**Supplementary Fig. 8a**,**b**). Pvalb expression correlates well with fast-spiking properties and basket-cell or axo-axonic morphology[3,33,39,40]. Sst is expressed in dendrite-targeting low-threshold rebound-spiking Martinotti cells, yet Martinotti cells are likely to represent only a subpopulation of Sst-expressing cells[35,38,41,42]. Vip expression is often found in irregular- and regular-spiking bipolar or double-bouquet cells[33,35,37]. We do not know whether our fourth category, the Tnfaip813-expressing cells, corresponds to a unique morphological or physiological type. Tnfaip813-expressing cells were labeled in the *Htr3a-GFP* line (**Supplementary Fig. 2**), which has been shown to also label neurogliaform cells[25,43]. As neurogliaform cells, the majority of Tnfaip813-expressing cells exhibited unspecific adapting firing properties (**Supplementary Fig. 8a**,**b**), suggesting a possible correspondence between these two cell types.

Irrespective of correlations of molecular with physiological or morphological parameters, our data show that the gene expression pattern is a strong predictor of connectivity between interneurons in the visual cortex, thus validating this categorization approach. Furthermore, a binary pattern simply based on the presence or absence of a transcript provides a simpler categorization criterion as compared to the quantitative analysis of electrophysiological characteristics or the often subjective morphological descriptions[19].

Comparison with previous studies

Although connectivity between molecularly identified interneurons in any cortical area has not been quantified systematically, several studies have addressed connectivity between specific types of interneurons using paired electrophysiological recordings or purely anatomical methods. Paired recordings have shown that fast-spiking cells (the electrophysiological correlate to Pvalb cells) in L2/3 and L4 are more likely to inhibit each other than to inhibit other interneurons and that the connectivity among fast-spiking cells is higher than the connectivity among other interneurons or from other interneurons onto fast-spiking cells[10,12,16]. Additional work has shown that morphologically identified Martinotti cells (a subtype of Sst cells) were the only class of L2/3 interneurons that substantially contacted L1 interneurons[15]. These reports are consistent with our data. Additional paired recordings in L2/3 established inhibitory connections originating from calretinin-expressing Vip cells onto fast-spiking, cells, Vip cells and cells that express calretinin but not Vip (calretinin-expressing non-Vip cells), as well as from calretinin-expressing non-Vip cells onto fast-spiking cells, Vip cells and calretinin-expressing non-Vip cells[11]. As calretinin expression partly overlaps with that of Sst[44], calretinin-expressing non-Vip cells might belong to the Sst cell category, and therefore the high connectivity rate for Vip cells onto calretinin-expressing non-Vip cells reported is consistent with our analysis. However, other reported connectivities (for example, the low conectivity of calretinin-expressing non-Vip cells onto pyramidal cells)[11] are inconsistent with the results reported here and await clarification. Finally, paired recordings have also shown that fast-spiking cells in L4 of somatosensory cortex inhibit low-threshold-spiking cells (putative Sst cells)[10,13,18]. The discrepancy with the data described here (Pvalb cells did not inhibit Sst cells) may be due to regional differences (visual cortex versus somatosensory cortex), layer specificity (L2/3 and L5 versus L4) or classification differences (whether Sst-expressing cells are exactly the same as low-threshold-spiking cells). Classification differences may also underlie the contrasting reports with regard to the presence[45] or absence[10,13,18] of synaptic connections between putative Sst cells.

Anatomical connections between identified or unidentified classes of interneurons have also been reported. Connections between Pvalb cells[9] and from Pvalb onto Vip cells[6,46] or from Vip onto Sst cells[8] have been observed in neocortex. Although not quantified in terms of strength or probability of occurrence, these anatomical observations are consistent with the present findings.

Functional implications

Pvalb and Sst cells target distinct subcellular compartments on pyramidal cells. Whereas Pvalb cells mainly inhibit the perisomatic compartments, Sst cells form synapses onto dendrites of pyramidal cells[2,4,5]. Given that Sst cells inhibit Pvalb cells, but not vice versa, one could imagine that activity in Sst cells will not only increase inhibition in the dendrites but also decrease Pvalb cell–mediated perisomatic inhibition. This could contribute to a shift of inhibition along the somatodenritic axis of pyramidal cells, similar to what has been described in the hippocampus[47]. In contrast to Pvalb and Sst cells, Vip cells inhibited pyramidal cells very little and specialized in the inhibition of Sst cells according to our data. Interneurons preferentially inhibiting other interneurons rather than pyramidal cells may be expected to be disinhibitory on pyramidal cells. But as Vip cells preferentially inhibited Sst cells and Sst cells inhibited Pvalb cells, active Vip cells, while decreasing Sst cell firing might, as a consequence, increase Pvalb cell firing. Thus, rather than disinhibiting pyramidal cells, Vip cells may shift inhibition back toward the soma.

The reciprocal connections among Pvalb cells but not Sst cells is another notable difference between the two cell types, which may allow Pvalb cells to control their own firing rate, as well as pace and synchronize each other during gamma oscillations[48].

The categorization of neuron types based on immunohistochemical characteristics[2,3] has been crucial for defining genetic strategies aimed at identifying, targeting, recording or manipulating distinct neuron categories[21,49]. Systematic whole-transcriptome analysis[50] of single cells, by vastly increasing the number of detected genes, will not only help refine our categorization criteria but eventually provide a causal link between the molecular expression patterns and the various functional and morphological properties of a given neuronal category. Nevertheless, despite the relatively limited amount of genetic markers used in this study, our observations suggest that the currently overwhelming complexity of connectivity patterns between cortical neurons may eventually be, at least in part, disambiguated based on the expression of a few genes.

METHODS

Methods and any associated references are available in the online version of the paper.

Note: Supplementary information is available in the online version of the paper.

ACKNOWLEDGMENTS

We thank J. Evora for help with genotyping and mouse husbandry, M. Chan for immunohistochemical labeling, J. Isaacson for critical reading of the manuscript and the members of the Scanziani and Isaacson laboratories for advice during

the course of the study. This work was supported in part by grants from the National Alliance for Research on Schizophrenia and Depression and US National Institutes of Health (NS047101). C.K.P. was supported by a European Molecular Biology Organization long-term fellowship (EMBO LTF 1114_2009) and the Howard Hughes Medical Institute. M.X. was supported by a fellowship from Jane Coffin Childs Memorial Fund for Medical Research. M.S. was supported by the Gatsby charitable foundation and the Howard Hughes Medical Institute.

AUTHOR CONTRIBUTIONS

C.K.P. and M.S. designed the study. C.K.P. conducted all experiments and analysis. M.X. contributed paired-recordings. Z.J.H. and M.H. contributed Vip-IRES-Cre mice. C.K.P. and M.S. wrote the paper.

COMPETING FINANCIAL INTERESTS

The authors declare no competing financial interests.

1. Isaacson, J.S. & Scanziani, M. How inhibition shapes cortical activity. *Neuron* **72**, 231–243 (2011).
2. Freund, T.F. & Buzsaki, G. Interneurons of the hippocampus. *Hippocampus* **6**, 347–470 (1996).
3. Kawaguchi, Y. & Kubota, Y. GABAergic cell subtypes and their synaptic connections in rat frontal cortex. *Cereb. Cortex* **7**, 476–486 (1997).
4. Markram, H. *et al.* Interneurons of the neocortical inhibitory system. *Nat. Rev. Neurosci.* **5**, 793–807 (2004).
5. Ascoli, G.A. *et al.* Petilla terminology: nomenclature of features of GABAergic interneurons of the cerebral cortex. *Nat. Rev. Neurosci.* **9**, 557–568 (2008).
6. Staiger, J.F., Freund, T.F. & Zilles, K. Interneurons immunoreactive for vasoactive intestinal polypeptide (Vip) are extensively innervated by parvalbumin-containing boutons in rat primary somatosensory cortex. *Eur. J. Neurosci.* **9**, 2259–2268 (1997).
7. Staiger, J.F. *et al.* Calbindin-containing interneurons are a target for Vip-immunoreactive synapses in rat primary somatosensory cortex. *J. Comp. Neurol.* **468**, 179–189 (2004).
8. Dalezios, Y. *et al.* Enrichment of mGluR7a in the presynaptic active zones of GABAergic and non-GABAergic terminals on interneurons in the rat somatosensory cortex. *Cereb. Cortex* **12**, 961–974 (2002).
9. Somogyi, P. *et al.* Salient features of synaptic organisation in the cerebral cortex. *Brain Res. Brain Res. Rev.* **26**, 113–135 (1998).
10. Gibson, J.R., Beierlein, M. & Connors, B.W. Two networks of electrically coupled inhibitory neurons in neocortex. *Nature* **402**, 75–79 (1999).
11. Caputi, A. *et al.* Two calretinin-positive GABAergic cell types in layer 2/3 of the mouse neocortex provide different forms of inhibition. *Cereb. Cortex* **19**, 1345–1359 (2009).
12. Galarreta, M. *et al.* Cannabinoid sensitivity and synaptic properties of 2 GABAergic networks in the neocortex. *Cereb. Cortex* **18**, 2296–2305 (2008).
13. Ma, Y., Hu, H. & Agmon, A. Short-term plasticity of unitary inhibitory-to-inhibitory synapses depends on the presynaptic interneuron subtype. *J. Neurosci.* **32**, 983–988 (2012).
14. Olah, S. *et al.* Output of neurogliaform cells to various neuron types in the human and rat cerebral cortex. *Front Neural Circuits* **1**, 4 (2007).
15. Jiang, X. *et al.* The organization of two new cortical interneuronal circuits. *Nat. Neurosci.* **16**, 210–218 (2013).
16. Avermann, M. *et al.* Microcircuits of excitatory and inhibitory neurons in layer 2/3 of mouse barrel cortex. *J. Neurophysiol.* **107**, 3116–3134 (2012).
17. Blatow, M. *et al.* A novel network of multipolar bursting interneurons generates theta frequency oscillations in neocortex. *Neuron* **38**, 805–817 (2003).
18. Hu, H., Ma, Y. & Agmon, A. Submillisecond firing synchrony between different subtypes of cortical interneurons connected chemically but not electrically. *J. Neurosci.* **31**, 3351–3361 (2011).
19. Defelipe, J. *et al.* New insights into the classification and nomenclature of cortical GABAergic interneurons. *Nat. Rev. Neurosci.* **14**, 202–216 (2013).
20. Hippenmeyer, S. *et al.* A developmental switch in the response of DRG neurons to ETS transcription factor signaling. *PLoS Biol.* **3**, e159 (2005).
21. Taniguchi, H. *et al.* A resource of Cre driver lines for genetic targeting of GABAergic neurons in cerebral cortex. *Neuron* **71**, 995–1013 (2011).
22. Fenno, L., Yizhar, O. & Deisseroth, K. The development and application of optogenetics. *Annu. Rev. Neurosci.* **34**, 389–412 (2011).
23. Lambolez, B. *et al.* AMPA receptor subunits expressed by single Purkinje cells. *Neuron* **9**, 247–258 (1992).
24. Xu, X., Roby, K.D. & Callaway, E.M. Immunochemical characterization of inhibitory mouse cortical neurons: three chemically distinct classes of inhibitory cells. *J. Comp. Neurol.* **518**, 389–404 (2010).
25. Lee, S. *et al.* The largest group of superficial neocortical GABAergic interneurons expresses ionotropic serotonin receptors. *J. Neurosci.* **30**, 16796–16808 (2010).
26. Kaneko, T. *et al.* Characterization of neocortical non-pyramidal neurons expressing preprotachykinins A and B: a double immunofluorescence study in the rat. *Neuroscience* **86**, 765–781 (1998).
27. Sugino, K. *et al.* Molecular taxonomy of major neuronal classes in the adult mouse forebrain. *Nat. Neurosci.* **9**, 99–107 (2006).
28. Vruwink, M. *et al.* Substance P and nitric oxide signaling in cerebral cortex: anatomical evidence for reciprocal signaling between two classes of interneurons. *J. Comp. Neurol.* **441**, 288–301 (2001).
29. Glickfeld, L.L. & Scanziani, M. Distinct timing in the activity of cannabinoid-sensitive and cannabinoid-insensitive basket cells. *Nat. Neurosci.* **9**, 807–815 (2006).
30. Fino, E. & Yuste, R. Dense inhibitory connectivity in neocortex. *Neuron* **69**, 1188–1203 (2011).
31. Packer, A.M. & Yuste, R. Dense, unspecific connectivity of neocortical parvalbumin-positive interneurons: a canonical microcircuit for inhibition? *J. Neurosci.* **31**, 13260–13271 (2011).
32. Williams, S.R. & Mitchell, S.J. Direct measurement of somatic voltage clamp errors in central neurons. *Nat. Neurosci.* **11**, 790–798 (2008).
33. Cauli, B. *et al.* Molecular and physiological diversity of cortical nonpyramidal cells. *J. Neurosci.* **17**, 3894–3906 (1997).
34. Galarreta, M. & Hestrin, S. A network of fast-spiking cells in the neocortex connected by electrical synapses. *Nature* **402**, 72–75 (1999).
35. Kawaguchi, Y. & Kubota, Y. Physiological and morphological identification of somatostatin- or vasoactive intestinal polypeptide-containing cells among GABAergic cell subtypes in rat frontal cortex. *J. Neurosci.* **16**, 2701–2715 (1996).
36. Kubota, Y. *et al.* Selective coexpression of multiple chemical markers defines discrete populations of neocortical GABAergic neurons. *Cereb. Cortex* **21**, 1803–1817 (2011).
37. Toledo-Rodriguez, M. *et al.* Neuropeptide and calcium-binding protein gene expression profiles predict neuronal anatomical type in the juvenile rat. *J. Physiol. (Lond.)* **567**, 401–413 (2005).
38. Wang, Y. *et al.* Anatomical, physiological and molecular properties of Martinotti cells in the somatosensory cortex of the juvenile rat. *J. Physiol. (Lond.)* **561**, 65–90 (2004).
39. Dumitriu, D. *et al.* Correlation between axonal morphologies and synaptic input kinetics of interneurons from mouse visual cortex. *Cereb. Cortex* **17**, 81–91 (2007).
40. Woodruff, A. *et al.* Depolarizing effect of neocortical chandelier neurons. *Front Neural Circuits* **3**, 15 (2009).
41. Ma, Y. *et al.* Distinct subtypes of somatostatin-containing neocortical interneurons revealed in transgenic mice. *J. Neurosci.* **26**, 5069–5082 (2006).
42. McGarry, L.M. *et al.* Quantitative classification of somatostatin-positive neocortical interneurons identifies three interneuron subtypes. *Front Neural Circuits* **4**, 12 (2010).
43. Vucurovic, K. *et al.* Serotonin 3A receptor subtype as an early and protracted marker of cortical interneuron subpopulations. *Cereb. Cortex* **20**, 2333–2347 (2010).
44. Xu, X., Roby, K.D. & Callaway, E.M. Mouse cortical inhibitory neuron type that coexpresses somatostatin and calretinin. *J. Comp. Neurol.* **499**, 144–160 (2006).
45. Reyes, A. *et al.* Target-cell-specific facilitation and depression in neocortical circuits. *Nat. Neurosci.* **1**, 279–285 (1998).
46. Staiger, J.F. *et al.* Innervation of interneurons immunoreactive for Vip by intrinsically bursting pyramidal cells and fast-spiking interneurons in infragranular layers of juvenile rat neocortex. *Eur. J. Neurosci.* **16**, 11–20 (2002).
47. Pouille, F. & Scanziani, M. Routing of spike series by dynamic circuits in the hippocampus. *Nature* **429**, 717–723 (2004).
48. Bartos, M., Vida, I. & Jonas, P. Synaptic mechanisms of synchronized gamma oscillations in inhibitory interneuron networks. *Nat. Rev. Neurosci.* **8**, 45–56 (2007).
49. Atallah, B.V. *et al.* Parvalbumin-expressing interneurons linearly transform cortical responses to visual stimuli. *Neuron* **73**, 159–170 (2012).
50. Tang, F. *et al.* mRNA-Seq whole-transcriptome analysis of a single cell. *Nat. Methods* **6**, 377–382 (2009).

ONLINE METHODS

Data collection and analysis. Data were collected and processed without randomization. Data collection was performed without blinding to the genotype of the mice. Data analysis was not blinded for overlap quantification of Cre lines. Electrophysiological analysis was done blinded to the gene expression of the cell and gene expression analysis was done blinded to the recorded inhibition of the cell.

Mice. Mice in this study were of mixed backgrounds (c57bl6, CD-1) and sexes and were group-housed in the vivarium under reversed light-dark (12 h and 12 h) conditions. The mice used had no previous history of drug administration, surgery or behavioral testing. All procedures were conducted in accordance with the US National Institutes of Health guidelines and with the approval of the Committee on Animal Care at the University of California, San Diego. Mice were used for experiments at postnatal ages (P)18–30. Transgenic mice used were: *Gad1*<tm1.1Tama> (Gad67-GFP; all subpopulations of interneurons)[51], Tg(*Gad*GFP)45704Swn (GIN; Sst cells)[52], Tg(*Gad1*-EGFP)G42Zjh (G42; Pvalb cells)[53], Tg(*Pvalb*-EGFP)B13Zjh (B13; Pvalb cells)[39], Tg(*Htr3a*-EGFP)DH30Gsat/Mmnc (Vip cells and others including layer 1)[25,43], *Gt(ROSA)26Sor*<tm14(CAG-tdTomato)Hze> (ROSA-tdTomato)[54], *Pvalb*<tm1(cre)Arbr> (Pvalb-Cre)[20], *Sst*<tm2.1(cre)Zjh> (SSt-Cre)[21]and *Vip*<tm1(cre)Zjh> (Vip-Cre)[21]. Mice used for experiments were heterozygous for the indicated genes.

Virus injection. Adeno-associated viruses (AAVs) for ChR2 were acquired from the University of Pennsylvania Viral Vector Core: AAV2/1.CAGGS.flex.ChR2.tdTomato.SV40 (Addgene 18917). Viruses were loaded in a beveled sharp micropipette mounted on a Nanoject II (Drumond) attached to a micromanipulator. ChR2 virus was injected into newborn pups (P0–P2) of Pvalb-Cre, Sst-Cre and Vip-Cre mice crossed to various GFP transgenic mice. Newborn mice were anesthetized on ice and secured into a molded platform. Three 23-nl boli of virus were injected unilaterally at each of three medial–lateral locations in V1 and three depths (450 μm, 300 μm and 150 μm).

Slice preparation. Mice were anasthetized with ketamine and xylazine (100 mg kg^{-1} and 10 mg kg^{-1}, respectively), perfused transcardially with cold sucrose solution (in mM: NaCl, 83; KCl, 2.5; $MgSO_4$, 3.3; NaH_2PO_4, 1; $NaHCO_3$, 26.2; D-glucose, 22; sucrose, 72; and $CaCl_2$, 0.5, bubbled with 95% O_2 and 5% CO_2) and decapitated, and the visual cortex was cut into 400-μm coronal sections in cold sucrose solution. Slices were incubated in sucrose solution in a submerged chamber at 34 °C for 30 min and then at room temperature (21 °C) until used for recordings.

Electrophysiology, photostimulation and cell collection. Whole-cell recordings were done at 32 °C in artificial cerebrospinal fluid (in mM: NaCl, 119; KCl, 2.5; NaH_2PO_4, 1.3; $NaHCO_3$, 26; D-glucose, 20; $MgCl_2$, 1.3; $CaCl_2$, 2.5; and mOsm, 305, bubbled with 95% O_2 and 5% CO_2). Whole-cell patch-clamp recordings were performed using pipettes with 2–5 MOhm resistance, and electrophysiological signals were amplified with a Multiclamp 700B amplifier (Axon Instruments), filtered at 2 kHz and digitized at 10 kHz or 50 kHz. Glass capillaries (Sutter) were baked at 200 °C before pulling pipettes to destroy RNases, washed several times with RNase-free water and RNase-free EtOH, dried and stored in a clean closed chamber. Inhibitory synaptic currents were recorded using either a cesium-based internal solution (in mM: $CsMeSO_4$, 115; NaCl, 4; HEPES, 10; Na_3GTP, 0.3; MgATP, 4; EGTA, 0.3; BAPTA(4Cs), 10; adjusted to pH 7.4 with CsOH; 295 mOsm) or a potassium-based internal solution (in mM: potassium gluconate, 134; $MgCl_2$, 1.5;HEPES, 10; EGTA, 0.1; magnesium ATP, 3; sodium phosphocreatine 10; adjusted to pH 7.4 with KOH; 295 mOsm). Internal solutions were prepared using RNase-free water and salts. Experiments were performed in the presence of the AMPA receptor antagonists NBQX (5 μM, Ascent, Asc-046) and of the $GABA_B$ receptor antagonist CGP54626 (1 μM, Tocris, 1088). Inhibitory postsynaptic currents using the Cs-based internal were recorded at +10 mV at which the contaminating photocurrent of occasionally recorded ChR2-expressing cells was negligible. Inhibitory postsynaptic currents using the K-based internal were recorded at −45 mV. The reversal potential for inhibition was −67 ± 2 mV ($n = 6$). Charges at +10 mV were ~8× larger (8.4 ± 0.9, $n = 6$) than charges measured at −45 mV (see charge-voltage relationship in **Supplementary Fig. 9a**). To combine recordings made at both potentials charges measured at −45 mV were therefore multiplied by 8. Current-clamp recordings were performed using the K-based internal solution. The spiking pattern and current-voltage characteristics of a neuron were determined immediately after achieving whole-cell configuration by a series of negative and positive current injections (800 ms). For assessing inhibition in postsynaptic neurons full-field photostimulation of ChR2-expressing interneurons consisted of single light pulses (2 ms) delivered by a 5-W blue LED (Thorlabs LEDC5), which was collimated and coupled to the epifluorescence path of an Olympus BX51 microscope. All experiments were carried out under an ×40, 0.8 numerical aperture (NA) water-immersion lens. Pairs made of a pyramidal cell and nearby GFP fluorescent interneuron were recorded in L2/3 or L5. For interneurons recorded in L1 the nearest upper L2 pyramidal cell was patched as reference. After recordings the interior of the interneuron was slowly sucked into the patch pipette. The content of the pipette was expelled into a precooled (−70 °C) safe-lock tube (Eppendorf; 1.5 ml) containing 1 μl RNase OUT (Invitrogen) and 4 μl RNAse-free water. The tube was centrifuged, snipped to mix the content and stored at −70 °C. Most of the recordings were terminated after 15 min. After each recording the pipette holder and silver wire were cleaned with RNase ZAP (Ambion, AM9780), RNase-free water and RNase-free EtOH. RNase-free gloves were used throughout experiments and frequently changed or cleaned with RNase-free EtOH. The tubes containing single-cell RNA were stored at −80 °C not longer than 3 months before further processing. Recordings were analyzed using Clampfit (Axon Instruments). The photostimulated postsynaptic currents used for the analysis were the average of ten sweeps. Charges represent the baseline subtracted time integral of the synaptic currents 5 ms before stimulus onset and 5 ms after the synaptic current returned to baseline. Because our 2-ms blue light stimulus triggers more than one spike in ChR2-expressing neurons (**Supplementary Fig. 8c–e**), our calculations of individual contributions of a given interneuron class onto other interneurons (**Figs. 4–7**) relied on the following assumption: that the short-term plasticity of transmitter release of a given interneuron class onto pyramidal cells is similar to that between that same interneuron class and other interneurons. This assumption is supported by observations that this is largely the case, at least for Pvalb, Sst and Vip cells[11,13,45] making our estimate of individual contribution between interneuron classes unlikely to be confounded by large differences of short-term plasticity. Most importantly, however, we confirmed our results obtained by photoactivation with paired recordings between identified interneurons (**Fig. 7**). The similarity of the results using both methods validated our approach. INC for each interneuron was calculated by dividing the IPSQ of the pyramidal cell with the average IPSQ measured using paired recordings of the respective interneuron onto pyramidal cell connection. The resulting number of presynaptic neurons (N_{pre}) was used to calculate the INC onto the respective interneuron ($INC_{IN} = IPSQ_{IN}/N_{pre}$). The INC for each postsynaptic interneuron class is the average over all individual INC values calculated for each recorded pair. INC data for interneurons recorded in L2/3 and L5 were pooled ($P > 0.1$ for the following combinations: Pvalb onto Pvalb, Sst, Vip, Tnfaip8l3, UD; Sst onto Pvalb, Sst, Vip, Tnfaip8l3, UD; Vip onto Pvalb, Vip, UD; Vip onto Sst $P = 0.043$), in case they were not statistically different (interneurons for the categories Vip and Tnfaip8l3 were largely confined to upper layers, therefore INCs represent mainly L2/3 measurements). To measure the inhibitory unitary connections, postsynaptic L2/3 pyramidal cells and L2/3 plus 5 interneurons (visualized by GFP fluorescence) were recorded under whole-cell voltage-clamp at +10 mV with the Cs-based internal solution, whereas nearby presynaptic interneurons (visualized by tdTomato expression in AAV-flexed-ChR2-tdTomato–injected Cre lines) were recorded under whole-cell current clamp with the K-based internal solution. Action potentials were elicited in interneurons by a 2-ms current injection (1–2 nA) with interstimulus interval of 15 s. uIPSQs were measured from the average of 10–50 sweeps. Values are given as mean ± s.e.m., if not otherwise indicated.

Immunohistochemistry, quantification of interneuron overlap. Triple transgenic mice (Pvalb-Cre, Sst-Cre, Vip-Cre, *ROSA-tdTomato*, *Gad67-GFP* and *Htr3a-GFP*) were anesthetized with ketamine and xylazine (100 mg kg^{-1} and 10 mg kg^{-1}, respectively) and perfused with phosphate-buffered saline (PBS, pH 7.4) and then 4% paraformaldehyde (PFA) in PBS, pH 7.4. After 2–3 h of incubation in PFA-PBS at 4 °C, brains were transferred in 30% sucrose solutions for at least 48 h at 4 °C. The visual cortex was cut into 50-μm coronal sections and mounted directly onto slides (for direct fluorescence analysis of GFP and tdTomato) or immunostained for Pvalb following standard protocols. In brief, free-floating sections were blocked with 2% normal goat serum, 1% BSA and 1% Triton X-100 in 0.1 M PBS. Dilutions of primary and secondary fluorophore-labeled

doi:10.1038/nn.3446

antibodies were applied in blocking solution. Sections were stained with primary antibody in the dark for at least 48 h at 4 °C slowly shaking and with secondary antibody at room temperature for 3–4 h. Antibodies used were rabbit anti-Pvalb (1:200, Abcam, Ab11427, see provider information for validation) and goat anti-rabbit AF633 (1:500, Invitrogen, A21070). Slices were mounted in Vectashield with DAPI (Vector Labs, H1500). Images were single confocal sections taken on an Olympus FV1000. Layer borders were identified by changes in cell density. Cell counts were carried out using standard stereological techniques. To calculate the overlap between interneuron specific Cre-lines the number of cells labeled by the respective Cre line and tdTomato (Pvalb-Cre, Sst-Cre and Vip-Cre), antibody staining (Pvalb-Cre) or GFP fluorescence (*Htr3a-GFP* and *Gad67-GFP*) was counted for each section as well as the number of co-labeled cells (double-fluorescent cells of Cre-tdTomato with Pvalb staining or Cre-tdTomato with GFP fluorescence in cells expressing GAD67-GFP or HTR3a-GFP, respectively) or the number of non-co-labeled cells (which was then subtracted from the number of stained cells to obtain the number of colabeled cells). Overlap was calculated dividing the number of colabeled cells by the number of the respective reference labeled cells (Cre-tdTomato–labeled cells, Pvalb stained cells, GAD67-GFP– or HTR3a-GFP–labeled cells). A small fraction of Pvalb, Sst and Vip cells did not overlap with the GFP expression pattern of the GAD67-GFP line. This discrepancy may be due in part because GFP may be expressed below our detection threshold in some interneurons and because a few Cre-expressing neurons may actually be glutamatergic. The presence of blockers for glutamatergic transmission in all electrophysiological experiments presented here excludes this potentially contaminating population from this analysis. Cre-tdTomato cells that did not show co-labeling with GAD67-GFP–labeled cells were excluded in the overlap quantification (mean ± s.e.m.; Pvalb-Cre–tdTomato: 10.2 ± 1.6%; Sst-Cre–tdTomato: 30.0 ± 3.1%; Vip-Cre–tdTomato: 23.0 ± 1.7%).

The distribution of neurons across layers was assessed by measuring the distance of each labeled cell to the pia and white matter and normalizing it to the distance between pia and white matter. Each neuron was then placed into ten equally spaced bins spanning the cortical slice and distributions were calculated based on these bins.

The quantification and overlap between the interneuron populations was carried out using Cre and reporter mice expressing their genes depending on the developmental time course of promoter activation. Our physiological measurements were done by injecting flexed ChR2-expressing virus postnatally (P0–P2). Hence, there may exist subtle differences between those methods regarding overlap quantification.

Single cell RT-PCR. Single cell RT-PCR was carried out using established procedures. First, a cDNA library of the transcriptome of the single cell was generated using oligo(dT) primers and the SuperScript III kit (Invitrogen, 18080-051) according to the manufacturer's protocol. Second, multiplex PCR was carried out with Accuprime Taq (Invitrogen, 12339-024) polymerase and primers for the 24 genes (**Supplementary Table 1**) using the entire cDNA library from step 1 in a volume of 100 µl. Multiplex primers were designed to amplify 400–600-bp exonic DNA sequences which spanned at least one exon-intron boundary. Multiplex PCR conditions were 60 °C annealing temperature with 2 min elongation time using 35–40 cycles. Third, nested single gene PCR was carried out in a volume of 25 µl with a 1:60 to 1:70 dilution of the multiplex PCR reaction using the standard Taq polymerase (Invitrogen, 18038-067). Nested primers were designed to amplify 200–400-bp DNA sequences within the multiplex PCR primer boundaries. Nested PCR conditions were 60 °C annealing temperature with 30-s elongation time using 35 cycles. PCR products were visualized and documented using standard agarose gel electrophoresis and SYBR-safe (Invitrogen, S33102) DNA staining with UV light. Primers were designed using Primer3Plus (http://www.bioinformatics.nl/cgi-bin/primer3plus/primer3plus.cgi) (**Supplementary Table 1**). Primers were tested with dilutions of cDNA libraries from mouse visual cortex (P20). PCR products were sequenced to check for nonspecific amplification of DNA. The final primer concentrations for multiplex and nested PCRs were ~1 µM. During scRT-PCR procedures, care was taken to eliminate RNase contamination and DNA cross-contamination. Water control experiments were regularly performed to control for traces of contamination. Thirty visually selected pyramidal cells were tested for amplification products of which in half of the scRT-PCRs Dlx6as1 primers were exchanged for vGluT1 primers (**Supplementary Fig. 6**). Gloves were changed frequently and different lab coats were worn for the different procedures and were regularly cleaned. These procedures assured contamination-free results. In our hands, contamination was not detectable, obviating the problem of false positives (see above and **Supplementary Fig. 6**). Missing detection of genes (false negatives) occurred in 5–10% of the samples (**Supplementary Fig. 3b**) Thus, a small fraction of neurons that should have been classified based on their primary or secondary markers to either Pvalb, Sst, Vip or Tnfaip8l3-expressing cells, may have been attributed to the undefined category or ended up in the discarded category and thus not further analyzed.

Postsynaptic interneuron categorization. Postsynaptic interneurons were categorized based on the expression of marker genes. Primary markers were selected based on largely mutually exclusive expression in single cells and coverage of a large fraction of interneurons. Secondary markers were selected based on the largely exclusive coexpression with one primary marker in single cells. Cells were categorized based on a simple scheme (**Fig. 2c**). The interneuron category is determined by the expression of primary markers. If only one primary marker was found, the cell was categorized according to this marker independently of secondary marker expression. If two primary markers are found (for example, *Pvalb* and *Sst*) the categorization depended on the presence of a secondary marker matching one of the two primary markers. These cells were attributed to the category corresponding to that primary marker that had a matching secondary. For example, *Tac1* was highly coexpressed in cells with *Pvalb* expression, thus cells expressing *Pvalb*, *Sst* and *Tac1* are classified as Pvalb. Cells with two primary markers but no matching secondary or more than two primary markers were excluded from the analysis (discarded). Cells without primary markers are categorized as undefined. Undefined cells in layer 1 were categorized as layer 1 (L1).

PCA and cluster analysis. Principal component analysis (PCA), *k*-means clustering and Ward's hierarchical tree clustering were performed using Statistica software (StatSoft, version 10).

PCA. Eigenvalues of principal components, coefficients of principal components (variables and genes) and eigenvectors (factor scores) of the cases (individual cells) were used to separate and cluster genes and cells. First, the scree plot (eigenvalues plotted against principal component number) was used to select the principal components that reduced the data drastically covering most of the variance. The first four principal components covered >50% of the variance with the last 20 components not adding substantially as visualized by the characteristic elbow shape of the curve (**Supplementary Fig. 4a**). The coefficients of principal components (weight factors, loadings) for the genes contributing to each of the principal components (PC1–4) were used to single out the most important genes carrying most of the variance. This was achieved by calculating the mean of all coefficients for PC1-4 in 4 dimensional Euclidean space and ranking the genes based on their distance from the mean. The most distant genes were further examined for strong coexpression with each other and the genes showing the least coexpression were selected (*Pvalb, Sst, Vip* and *Tnfaip8l3*; *Nxph1* was eliminated because of strong overlap with *Pvalb, Sst* and *Tnfaip8l3*). To additional further genes that exhibited the least variance to the primary selected genes we calculated the Euclidean distances in four-dimensional space (PC1–4) for each primary gene to all other genes and selected the closest genes in Euclidean space (**Supplementary Fig. 4b**,**c**). This gave us the reduced selection of primary (*Pvalb, Sst, Vip* and *Tnfaip8l3*) and secondary (*Tac1, Grin3a, Pdyn, Tac2* and *Sema3c*) marker genes to separate most of the cells covering most of the variance. We used these primary and secondary markers to cluster the cases (cells) into 6 groups (Pvalb, Sst, Vip, Tnfaip8l3, discarded, undefined) according to the rules described above (**Fig. 2c**). The overlap of cells of different classes in four-dimensional Euclidean space (PC1–4) was calculated using the eigenvectors (factor scores) of the first four principal components (PC1–4). We calculated the overlap in two ways. First, we compared the Euclidean distance between each cell of two separate classes with the Euclidean distance to the nearest neighbor within the same class. If the distance of a cell from class A to the closest cell within the same class was bigger than to a cell from class B, the cell from class B would overlap with class A. Second, we calculated the overlap of vectors of cell A and B (dot product of vectors divided by length of vector A) in four-dimensional Euclidean space between the cells of two separate classes. If the overlap of the vector of a cell from class A to the nearest neighbor within the same class was smaller than the overlap in vector space to a cell from class B, the cell from class B would overlap with class A. The two methods of calculating the overlap gave very

similar results, of which the distance related overlap calculations are depicted in **Supplementary Figure 4e**.

k-*means clustering*. We performed *k*-means centroid–based clustering by setting the initial cluster number to 6. Cells were separated accordingly into 6 clusters (**Supplementary Fig. 5a**). The cells in each cluster were then compared to the cells in clusters defined by PCA or expression analysis.

Joining tree clustering. Tree-based hierarchical clustering was applied using the Ward's algorithm to select for variables (genes) showing strongest or least separation (**Supplementary Fig. 5b**).

Statistics. Statistical comparisons were performed using the nonparametric two-sided Mann-Whitney test and are given as *P* values. $P < 0.05$ was interpreted as statistically different. All other values are given as mean ± s.e.m. No statistical methods were used to predetermine sample sizes, but our sample sizes are similar to those reported in previous publications in the field[12,16].

51. Tamamaki, N. *et al*. Green fluorescent protein expression and colocalization with calretinin, parvalbumin, and somatostatin in the GAD67-GFP knock-in mouse. *J. Comp. Neurol.* **467**, 60–79 (2003).
52. Oliva, A.A. Jr. *et al.* Novel hippocampal interneuronal subtypes identified using transgenic mice that express green fluorescent protein in GABAergic interneurons. *J. Neurosci.* **20**, 3354–3368 (2000).
53. Chattopadhyaya, B. *et al.* Experience and activity-dependent maturation of perisomatic GABAergic innervation in primary visual cortex during a postnatal critical period. *J. Neurosci.* **24**, 9598–9611 (2004).
54. Madisen, L. *et al*. A robust and high-throughput Cre reporting and characterization system for the whole mouse brain. *Nat. Neurosci.* **13**, 133–140 (2010).

doi:10.1038/nn.3446